Polarized light scattering from metallic particles on silicon wafers

Jung Hyeun Kim,[a,b] Sheryl H. Ehrman,[b] George W. Mulholland,[a] and Thomas A. Germer[a]

[a]*National Institute of Standards and Technology, Gaithersburg, MD 20899*
[b]*Department of Chemical Engineering, University of Maryland, College Park, MD 20742*

ABSTRACT

Polarized light scattering by monodisperse copper and gold spheres, having diameters ranging from 96 nm to 205 nm, deposited on silicon substrates were measured using visible light. The results are compared to an exact theory for scattering by a sphere on a surface, originally developed by Bobbert and Vlieger. The results show that accurate calculation of the scattering of light by a metal sphere requires that the near-field interaction between the sphere and its image be included in a complete manner, that the normal incidence approximation does not suffice for this interaction, and that the existence of any thin oxide layer on the substrate must be included. The polarization of light scattered by these spheres on silicon substrates can be used to determine the size of those spheres. However, uncertainties in the thickness of the substrate oxide layer, roughness of the particles, and uncertainties in the optical properties of the particles may prevent them from being used as standard scatterers. The implementation of the theory, which requires special care when the spheres are metallic and the substrate is highly reflecting, is described in detail.

Keywords: copper, gold, inspection, metal, particles, polarization, scattering, spheres

1. INTRODUCTION

Light scattering is used by the semiconductor, optical, and data storage industries to inspect materials for surface quality.[1] The development of more sensitive and accurate tools requires understanding the scattering behavior of the different types of defects that the tools are expected to encounter. Theoretical models, validated by well-characterized measurements, enable manufacturers to predict and optimize the performance of their tools. While numerous studies have investigated the scattering of light by small dielectric spheres,[2–7] and while such spheres are often used for calibrating scanning surface inspection systems, the scattering from such spheres does not necessarily behave like that from real production line particle defects. Furthermore, the scattering from metallic particles is complicated by the much stronger near-field interaction between the particle and the substrate, placing larger demands on the theoretical models. The development and validation of a robust scattering theory for a sphere on a substrate creates a benchmark by which approximate codes for arbitrarily-shaped structures can be tested.[4,8]

Recently, several studies have shown that the polarization of scattered light can be used to characterize and distinguish amongst different types of defects, such as particulate contaminants,[9] surface roughness,[10,11] and subsurface defects.[9,10] In this paper, we present measurements and theoretical calculations for light scattering from copper and gold spheres deposited on silicon surfaces. The polarization state and the differential scattering cross-section (DSC) for light scattering from particles having diameters ranging from 96 nm to 205 nm have been measured using a Goniometric Optical Scatter Instrument (GOSI) as functions of incident angle, polar scattering angle, and out-of-plane scattering angle, using polarized, visible laser light. Theoretical calculations, based on the theory of Bobbert and Vlieger[12] (BV), are compared to the data. By comparing the scattering behavior to that predicted by other approximate models, namely the Mie-surface double interaction model[2] (MSDI) and the Videen normal incidence approximation[13,14] (NIA), we gain insight how different aspects of the scattering are controlled by different parameters of the particles. As expected, metal particles show a more complicated interaction with the silicon substrate than do dielectric particles.

The sample-scattering coordinate system we use for light scattering measurements and theoretical calculations is shown in Fig. 1(a). The schematic diagram defining the parameters of the scattering model for the scattering by a sphere above a surface is shown in Fig. 1(b). In Sec. 2, the theory of Bobbert and Vlieger and our implementation of it are described. In Sec. 3, we describe the sample preparation and the experimental procedures for the scattering measurements. In Sec. 4, we present and discuss the results. Finally, we summarize the paper in Sec. 5.

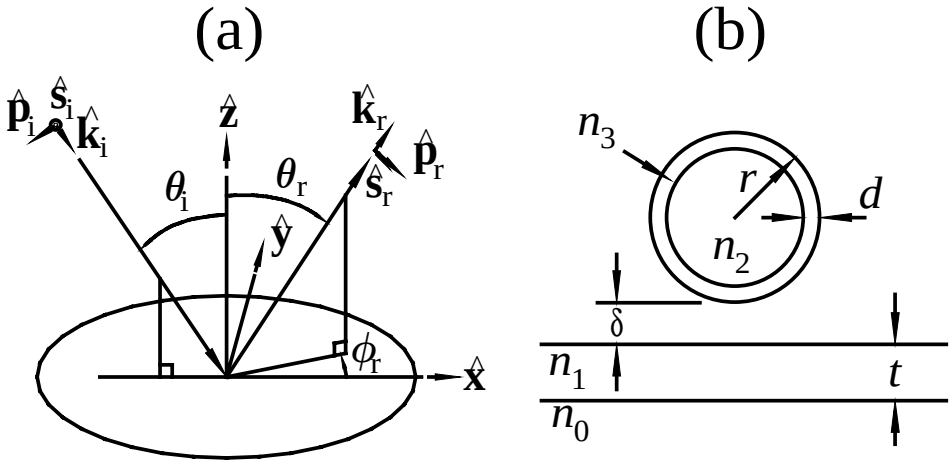

Figure 1. (a) The sample coordinate system used in this study, and (b) a schematic diagram of a particle on a substrate. In (b), n_0, n_1, n_2, and n_3 are the indices of refraction for the substrate, substrate coating, particle, and particle coating, respectively. The substrate coating thickness is t, d is the particle coating thickness, and δ is the distance between substrate and particle.

2. THEORY

An exact solution to the scattering of light by a sphere above a surface was found by Bobbert and Vlieger (BV).[12] Using an extension of Weyl's method for the reflection of dipole radiation by a flat surface, they derive the reflection matrix using the Debye potentials used in the Mie scattering problem as the basis. The Mie scattering solution for a sphere in free space can be represented as a matrix **B** relating the incident field, represented by a vector **V**, to the scattered field, represented by a vector **W**. A reflection matrix **A** relates the scattered field to that reflected back from the surface. The total scattering matrix is then shown to be given by

$$(\mathbf{1}-\mathbf{B}\cdot\mathbf{A})^{-1}\cdot\mathbf{B}\,. \tag{1}$$

Thus, they are able to self-consistently include the presence of the partially reflecting plane in the Mie solution. Bobbert, Vlieger, and Greef[15] (BVG) presented the numerical methods used to evaluate the theory for mercury spheres above a carbon substrate in an aqueous surrounding. Convergence of the solution is most rapid for surfaces or spheres having indices near unity. Since the relative index of the spheres (Hg) compared to the surrounding (H_2O) was $1.44 + 4.11i$, while that of the substrate (C) was $1.47 + 0.60i$, convergence was quick in their study. In contrast, the solution for a noble metal sphere, such as copper or gold, on a high-index substrate, such as silicon, in an ambient air environment does not converge rapidly at all. The numerical approaches described by BVG do not behave well for these poorly converging solutions. Therefore, in producing a computer code that implements the BV theory, we have made a number of changes and learned a number of lessons:

1. In the free space Mie scattering problem, Bohren and Huffman[16] (BH) suggest truncating the series in angular momentum by

$$l_m = q + 4q^{1/3} + 2\,, \tag{2}$$

where $q = 2\pi r/\lambda$ and r is the radius of the sphere and λ is the wavelength of light. They warn their readers that continuing much beyond this point leads to trouble due to their use of recursion relationships in the evaluation of the spherical Bessel functions. For scattering near a surface, especially for the case of a copper or gold sphere on silicon, the series in l does not converge until substantially beyond that given by Eq. (2). For this reason, it is crucial to heed the warning of BH and not use recursion relationships to calculate the spherical Bessel functions for orders much higher than the argument. At these values, the Taylor series formula of the Bessel function is adequate and converges rapidly:

$$J_n(z) = (z/2)^n \sum_{i=0}^{\infty} [-(z/2)^2]^i / [i!\Gamma(n+i+1)]\,. \tag{3}$$

2. BVG use a 50-node Gaussian rule appropriate for the integration of the product of a decaying exponential and a slowly varying function. We found, however, that such integration does not perform well for higher order terms of the matrix. We

choose instead to numerically evaluate the infinite integral in BV's Eq. (8.17) by piecewise integration. The integral, as pointed out by BV, is of the form

$$\int_1^{i\infty} d(\cos\alpha) e^{2iq\cos\alpha} r(\cos\alpha)\, p(\cos\alpha)\,, \tag{4}$$

where $r(\cos\alpha)$ is a reflection coefficient and $p(\cos\alpha)$ is a polynomial in $\cos\alpha$. The indefinite integral

$$\int d(\cos\alpha) e^{2iq\cos\alpha} (\cos\alpha)^n \tag{5}$$

can be solved exactly, and its solution is given by

$$\frac{-n! e^{2iq}}{2iq} \sum_{j=0}^{n} \frac{(-1)^j}{(n-j)!(2iq)^j}\,. \tag{6}$$

The function $r(\cos\alpha)$ is not a polynomial and has most of its structure near $\cos\alpha = 1$, with little structure as it approaches $i\infty$. Therefore, we perform piecewise cubic interpolation of $r(\cos\alpha)$ over a relatively small number of regions (5—15) over the range $\cos\alpha = 1$ to $iC_{\max}$ (with $C_{\max}$ between 20 and 45). The relative size of each interpolation piece is chosen adaptively to place smaller pieces in regions with more structure, in an effort to minimize errors in the interpolation of $r(\cos\alpha)$. The last piece of the integral is evaluated to $i\infty$ using $r(\cos\alpha) = r(i\infty)$. Having interpolated the reflection coefficient as a polynomial, the piecewise integral can be readily performed. By writing code to perform polynomial arithmetic, the code manipulates the Legendre polynomials, the rotation matrix elements [$d^l_{m,m'}(\alpha)$ in BV], and their associated products as arrays of polynomial coefficients, using Eq. (6) to evaluate the result at the end.

3. The scattered field can be written in the separated form

$$E_{jk} = \sum_{l=1}^{l_m} \sum_{m=-l}^{l} W_{lm}(\theta_i, j) Z_{lm}(\theta_r, k) \Phi_m(\phi_r) \tag{7}$$

where j and k represent the incident and scattering polarizations, respectively. Separating E_{jk} into this form speeds the evaluation of the scattering function at multiple angles, especially, if one angle is held fixed. Furthermore, once calculation of the scattering wave $W_{lm}(\theta_i, j)$ is achieved, it is found that only terms up to l_m given by Eq. (2) need to be included in the summation. This substantially increases the speed of evaluating the scattering function over multiple scattering directions, such as is needed to evaluate, for example, the total scattering cross section.

4. For large l_m, the matrix inverse of $\mathbf{1 - B \cdot A}$ does not behave well numerically. It was found that the inverse of **C**, where $\mathbf{C = B^{-1} (1 - B \cdot A)}$, is substantially better behaved, but eventually accumulates large errors that propagate to the final solution of the scattering problem. It has been found, however, that iterative improvement[17] of the solution can be achieved by applying the transformation

$$\mathbf{W} \leftarrow \mathbf{W} - \tilde{\mathbf{C}}^{-1} \cdot [\mathbf{C} \cdot \mathbf{W} - \mathbf{V}] \tag{8}$$

a couple of times, where $\tilde{\mathbf{C}}^{-1}$ is the matrix inverse of **C**, obtained numerically.

5. The theory described by BV applies to any spherically symmetric particle above any planarly symmetric substrate. The presence of a coating on the sphere can be incorporated into the theory by replacing the formula for the Mie scattering matrix **B** by an appropriate matrix for a coated sphere, such as that given by BH Sec. 8.1.[16] Furthermore, the substrate reflection matrix **A** is given in BV with respect to the reflection coefficients of the substrate, $r_s(\cos\alpha)$ and $r_p(\cos\alpha)$. The presence of a substrate coating can be incorporated into the theory simply by using the reflection coefficients appropriate for a coated substrate. Lastly, BV take the limit as the spacing between the substrate and the particle, δ, approaches zero. It is readily apparent that the size parameter q for the calculation of the matrix **B** is derived from the size of the particle, while that for reflection matrix **A**, incident plane wave vector **V**, and the function $\Theta_{lm}(\theta_r, k)$, q is derived from the distance of the center of the particle to the surface. As an aside, the presence of a low index coating on the substrate or the sphere, or a non-zero δ substantially improves the rate of convergence.

6. The matrix **A** needs to be calculated only once for a given substrate and sphere-substrate distance, $r + \delta$. If one is checking for convergence, it is advantageous to calculate the scattering matrix **A** for l_m much larger than anticipated, and use parts of it for smaller l_m. Once must still invert the matrix $\mathbf{C} = \mathbf{B}^{-1} (\mathbf{1} - \mathbf{B} \cdot \mathbf{A})$, but most of the computation time is in the calculation of the matrix **A**.

Following the steps outlined above allows the scattering to be calculated to an arbitrary level of accuracy. Our implementation of the code has been written in C++, and is encapsulated in a form suitable for inclusion in the SCATMECH library of scattering models developed by NIST and available on the Internet.[18] The computation time of our implementation of the BV theory scales as approximately $l_m^{3.6}$. The free storage memory requirements are approximately 100 kB per unit change of l_m.

Two approximations that are commonly used in scattering calculations are the Mie-surface double interaction (MSDI) model of Nahm and Wolfe and the normal incidence approximation (NIA) of Videen. The MSDI model can be evaluated using the BV theory by ignoring the interaction of the sphere with its image in the substrate, that is, by making the approximation $\mathbf{A} = 0$. The NIA model can be evaluated by letting the reflection coefficients be given by their normal incidence values, allowing the integrals of the form given by Eq. (4) to be performed exactly.

3. EXPERIMENT

3.1. Sample Preparation

Copper spheres were deposited onto wafers from an aerosol. Solution droplets containing copper nitrate were generated by nebulization using compressed nitrogen, and were carried by nitrogen gas into a high temperature furnace (1000 °C). The solvent evaporated and the copper nitrate residue particles decomposed in the presence of the vaporized solvent to produce pure copper particles. The detailed mechanism of pure copper formation will be described elsewhere.[19] The particles were size-classified[20] from the polydisperse aerosol using a bipolar charger and a differential mobility analyzer (DMA) operated at specific applied voltage and flow conditions to yield particles of diameters 96 nm, 113 nm, 144 nm, 158 nm, and 198 nm. The classified particle sizes were also measured by transmission electron microscopy (TEM). The mean diameter of particles classified to be 100 nm by the DMA were found to be 101 nm as measured by the TEM. An electrostatic precipitator connected to the particle generation and classification system was used to deposit the monodisperse copper spheres onto bare silicon wafers. We used a dark field optical microscope to count deposited particles to determine the particle number density. The resulting particle densities were[21] $(900 \pm 80)\ \mathrm{mm}^{-2}$ for 96 nm particles, $(900 \pm 70)\ \mathrm{mm}^{-2}$ for 113 nm particles, $(300 \pm 20)\ \mathrm{mm}^{-2}$ for 144 nm particles, $(350 \pm 30)\ \mathrm{mm}^{-2}$ for 158 nm particles, and $(170 \pm 20)\ \mathrm{mm}^{-2}$ for 198 nm particles. The index of refraction of copper used for the model calculations was $n_{Cu} = 0.249 + 3.41i$ at $\lambda = 633$ nm.[22]

Gold spheres were deposited onto wafers using a wet chemical process. Clean wafers, whose oxide surfaces have hydroxyl functionality, were immersed in a solution containing (3-mercaptopropyl) trimethoxysilane (MPTMS) (United Chemical Technologies[23]). The wafers experience a condensation reaction with MPTMS, whereby the surfaces become covered with organosilane sulfhydryl groups. The wafers were then immersed into solutions containing gold colloidal solutions (BBInternational[23]), having particles with mean diameters of 98 nm, 155 nm, and 205 nm. The gold spheres react with the surfaces to form strong covalent bonds.[24] The concentration of particles in the solution determines the final density of spheres on the surface. The particle densities of the samples prepared for scattering experiments were[21] $(33\,000 \pm 1\,000)\ \mathrm{mm}^{-2}$ for a mean diameter of 98 nm, $(35\,000 \pm 1\,000)\ \mathrm{mm}^{-2}$ for a mean diameter of 155 nm, and $(23\,000 \pm 1\,000)\ \mathrm{mm}^{-2}$ for a mean diameter of 205 nm. In model calculations, we used the literature value[22] for the index of refraction of gold, $n_{Au} = 0.467 + 2.415i$, at $\lambda = 532$ nm. The presence of the organosilane layer contributed to the background scattering level of the wafer, especially in near specular directions, and necessitated the use of higher particle densities. The gold particle diameters were distributed over a range approximately 5 % above and below their mean diameter.

Prior to depositing any particles, all wafers were cleaned with the RCA cleaning procedure[25] and checked by light scattering. The bidirectional reflectance distribution function (BRDF) from a well-cleaned wafer was about $4 \times 10^{-8}\ \mathrm{sr}^{-1}$ at the wavelength $\lambda = 633$ nm and for typical non-specular geometries. The quality of silicon substrates is critical in order to test scattering models with low densities of particles. All cleaned wafers were assumed to have an approximately 2 nm thick native oxide layer, typical for wafers exposed to air.[26]

3.2. Optical Scattering Measurements

The optical scattering geometry used for in-plane and out-of-plane measurements is shown in Figure 1(a). The Goniometric Optical Scatter Instrument (GOSI), described elsewhere,[27,28] was used to perform the measurements. We selectively used laser light of wavelength λ = 633 nm for the copper spheres and λ = 532 nm for the gold spheres. Different wavelengths were used for the two particle materials due to the timing of the measurements with other measurements being performed by the instrument. The laser spot size was approximately 1 mm in diameter. Measurements were performed both in the plane of incidence and out of the plane of incidence. Specific incident polarizations were chosen to yield high differentiation amongst different particle sizes. Out-of-plane measurements were performed using p-polarized incident light with fixed incident angle θ_i and scattering angle θ_r (= θ_i), scanning the azimuthal angle ϕ_r. In-plane measurements were performed using 45° incident polarization using a fixed incident angle θ_i, scanning the viewing angle θ_r. In all measurements, the scattered light was analyzed for polarization state using a rotating-compensator-fixed-polarizer arrangement. The DSC is related to the measured BRDF by

$$\mathrm{DSC} = \mathrm{BRDF} \cdot \cos(\theta_r) / \rho \,, \tag{9}$$

where ρ is the particle density. The polarization state of the light is parameterized by its principal angle of polarization η, its degree of circular polarization P_C, and its total degree of polarization P. Since some depolarization was observed in the data, we show the normalized degree of circular polarization P_C/P. The normalized value represents the degree of circular polarization of the fraction of light which is polarized, since all of the theories predict P = 1. While a complete uncertainty analysis has not been performed for these measurements, the uncertainties in DSC, η, P_C, and P are expected to be dominated by statistical sources and can be estimated by observing the point-to-point variation in the data.

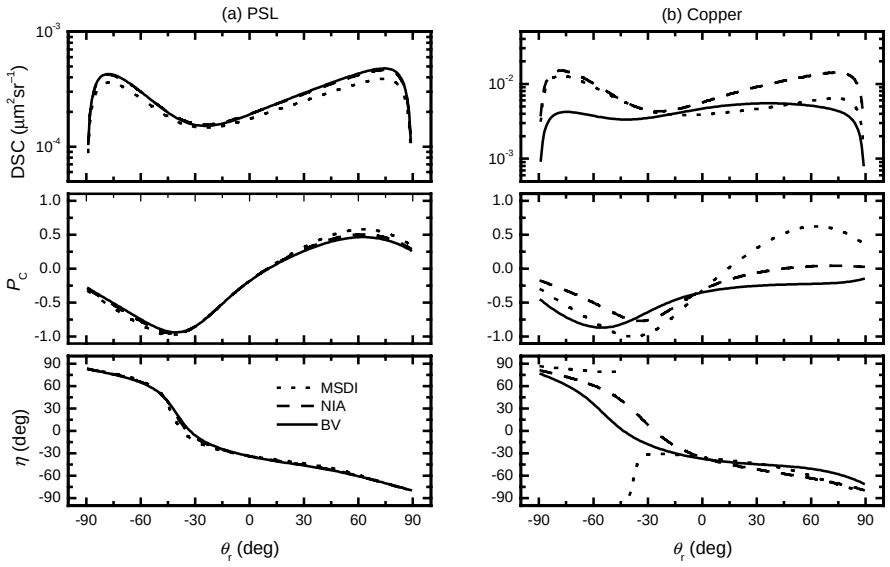

Figure 2. Light scattering parameters for a sphere on a silicon substrate predicted by the MSDI model, NIA model, and the BV theory in the plane of incidence for θ_i = 45° and at λ = 633 nm: for (a) a 150 nm PSL sphere, and (b) for a 150 nm copper sphere.

4. RESULTS AND DISCUSSION

Figure 2 shows a comparison of the MSDI model, NIA model, and the BV theory for 150 nm polystyrene latex (PSL, index n_{PSL} = 1.59) and copper spheres on a silicon wafer using λ = 633 nm. The three theories predict similar behaviors for the PSL sphere, indicating that the near-field interaction between the sphere and the substrate, which is ignored in the MSDI model and incompletely treated in the NIA model, is weak. In comparison, the three theories predict very different results for the copper sphere, where the sphere-surface interaction is much stronger. The failure of the NIA model further suggests that large wavevectors contribute to the near-field interaction. This finding is consistent with the very slow convergence of the

BV theory for copper, requiring values of l_m on the order of 30 to 60, compared to 7 to 10 for PSL. The slow convergence also suggests that the scattering will be very sensitive to the shape of the particle, i.e., if it is not spherical. The use of the full BV theory is clearly necessary when comparing data to theoretical calculations.

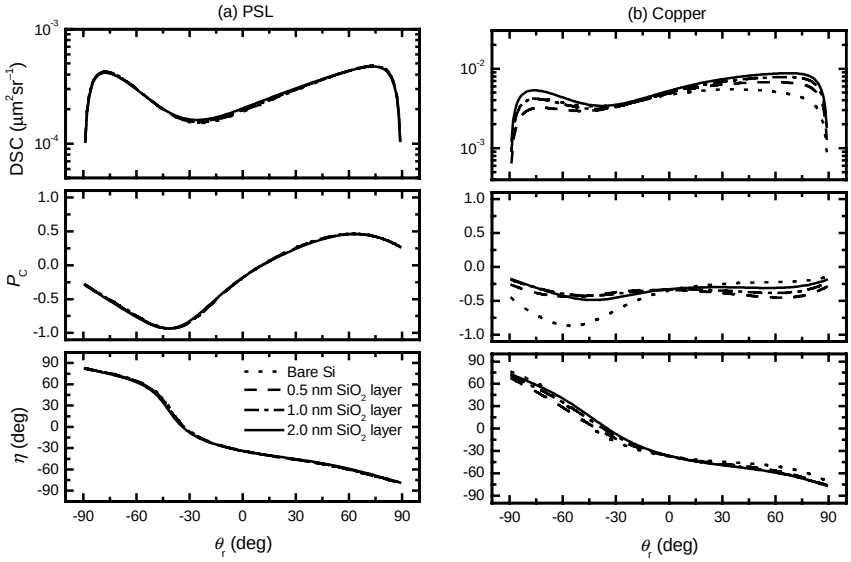

Figure 3. Light scattering parameters for a sphere on a silicon substrate predicted by the BV theory for different SiO_2 layer thicknesses, calculated in the plane of incidence for $\theta_i = 45°$ and λ=633 nm: for (a) a 150 nm PSL sphere, and (b) for a 150 nm copper sphere.

The scattering from metal spheres on a surface depends very strongly on the existence and thickness of any dielectric layer on the substrate. Figure 3 shows a comparison of the BV theory for scattering from PSL and copper spheres on thin SiO_2 layers on the substrate, with thicknesses ranging from t = 0 nm to 2 nm. These thicknesses are thin enough that they are nearly imperceptible to any far field reflection measurement. The scattering from PSL spheres is relatively unperturbed by the existence of such a layer. However, the effects of the layer are significant for the copper spheres, with the DSC changing by more than a factor of two at some angles and the polarization state being significantly perturbed. The implications of this strong thickness dependence are interesting. Near-field scattering probes are the subject of a great deal of current literature and rely upon this sensitivity to obtain subwavelength optical characterization of surface features.[29,30] As a scattering standard, however, it poses a problem: the scattering from metallic spheres depends much too strongly on the condition of the surface on which it rests to reliably provide a stable scattering source. In the theory-experiment comparisons that follow, the existence of a 2 nm native oxide layer on the silicon substrate is included in the calculations.

Figure 4 shows the light scattering parameters for samples with 96 nm, 113 nm, and 158 nm copper spheres measured out of the plane of incidence for (a) $\theta_i = \theta_r = 45°$ and (b) $\theta_i = \theta_r = 60°$ at λ = 633 nm. The agreement between the measured principal polarization angles η, the normalized degree of circular polarization P_c/P , and the DSC with those predicted by the BV theory is excellent. The largest deviations were observed for the larger particles (158 nm), for which a high degree of depolarization (P < 1) is observed. As noted above, the theory suggests a strong dependence on particle shape, and the largest particles may exhibit a small amount of surface roughness, rendering them non-spherical. Such non-sphericity will contribute a random component to the scattering, lowering the degree of polarization. Despite the degree of depolarization, the normalized degree of circular polarization P_c/P seems to agree with the theory very well.

Figure 5 shows the light scattering parameters measured in the plane of incidence using 45°-polarized light of wavelength λ = 633 nm for the same three sizes of copper spheres and for θ_i= 45° and θ_i= 60°. The agreement between the measured data and the predictions of the BV theory is very good, as we have seen with the out-of-plane measurements. The omitted data in the graphs are in regions where the specular reflection dominates the scatter (θ_r near θ_i) or where the receiver obscures the incident light (θ_r near $-\theta_i$). Some deviation from the theory is observed at large angles ($|\theta_r| > 75°$). At this time, we do not understand the source of this deviation, and it may be a result of an instrumental artifact.

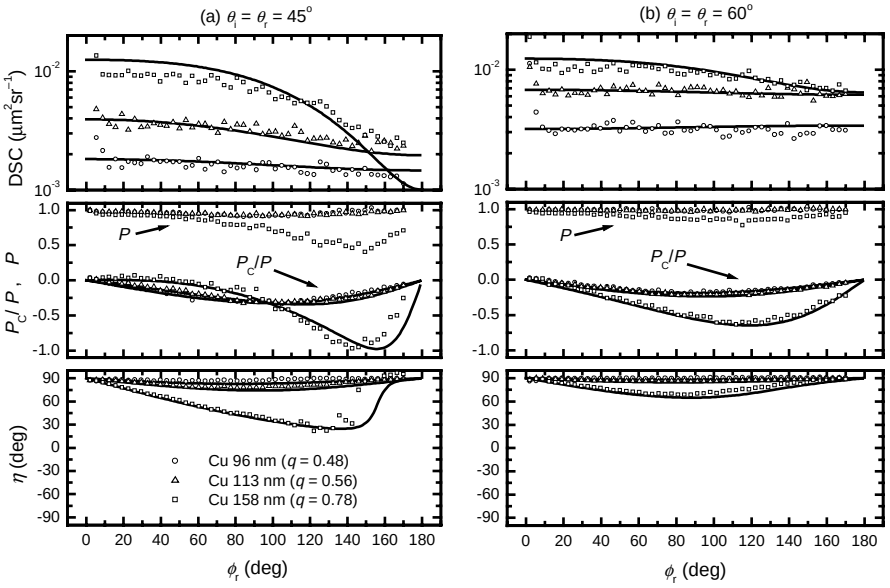

Figure 4. Light scattering parameters for 96 nm, 113 nm, and 158 nm copper spheres measured out of the plane of incidence for λ = 633 nm and for (a) $\theta_i = \theta_r = 45^o$, and (b) $\theta_i = \theta_r = 60^o$. The solid curves represent the predictions of the BV theory.

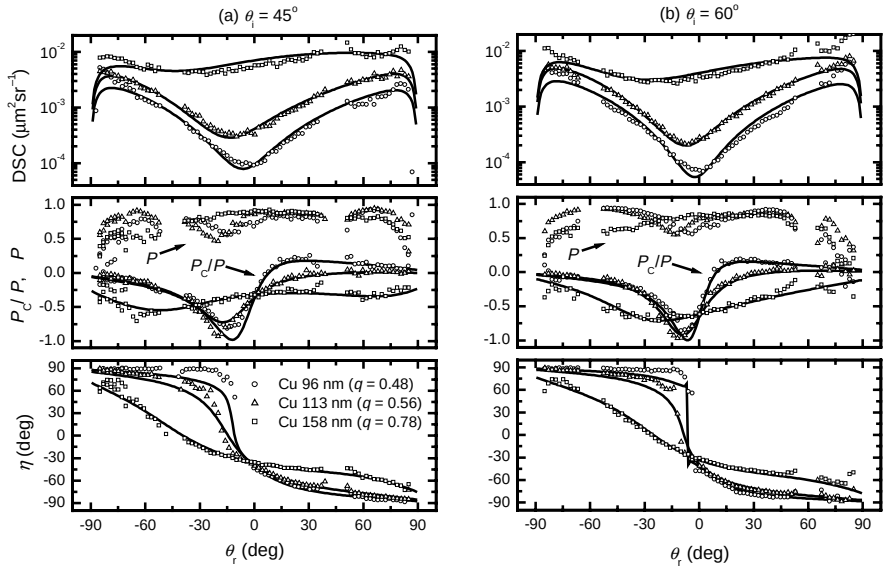

Figure 5. Light scattering parameters for 96 nm, 113 nm, and 158 nm copper spheres measured in the plane of incidence for λ = 633 nm and for (a) $\theta_i = 45°$, and (b) $\theta_i = 60°$. The solid curves represent the predictions of the BV theory.

Figure 6 summarizes the results for gold particles measured with λ = 532 nm. In Fig. 6(a), out-of-plane scattering data for the three different sizes (98 nm, 155 nm, and 205 nm) of gold spheres are shown for $\theta_i = \theta_r = 45°$. The agreement between the experimental data and the theory is good, but significant depolarization is observed for the smallest particle size (98 nm). Furthermore, at small scattering angles, the scattering is dominated by the presence of the inhomogeneous organosilane layer. Additional considerations include the presence of some gold clusters on the surface, as observed with dark field microscopy, and the possibility of multiple scattering arising from the high particle densities used in these measurements. Figure 6(b) shows data for the 205 nm gold spheres measured in different geometries. The trends in the data behave very

similar to the predictions of the BV theory. The large deviation observed in η near $\phi_r = 70°$ is a result of the large degree of circular polarization P_C at these angles; when P_C is near 1 or –1, the principal angle η is not well defined.

In a previous study,[5] it was found that the size of a particle can be estimated from the rate at which η changes as one changes ϕ_r near the specular direction for p-polarized incident light. The basis for this interpretation followed from the predictions of a Rayleigh scattering model, which yielded very similar predictions to that from more accurate models. Since the Rayleigh model did not account for the sphere material, it was believed that this behavior was associated with the size of the sphere. Thus, one could estimate the size of the particle by measuring $-d\eta/d\phi_r$ near the specular direction. Figure 7(a) shows a graph for the extracted values of the initial slope $-d\eta/d\phi_r$ obtained from the experimental data (in Figs. 4 and 6) and the BV theory for copper and gold and the Rayleigh theory. The uncertainties ($\pm 2\sigma$) were evaluated by standard statistical data analysis from the linear regression of data in the low ϕ_s region. The measured values for gold and copper spheres are in good agreement with the BV predictions. The differences between the BV theory and the Rayleigh approximation underline the need to use the full theory for metallic particles.

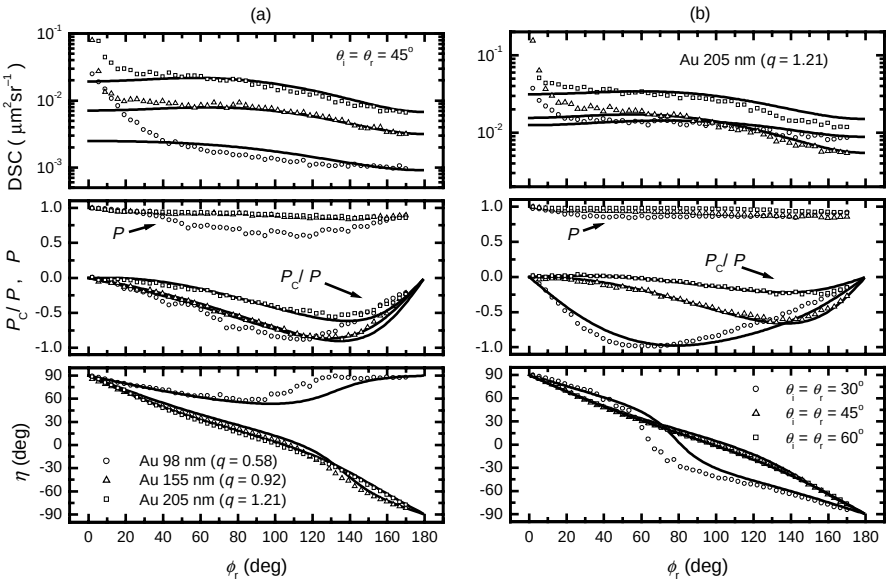

Figure 6. Light scattering parameters for gold spheres measured out of the plane of incidence for $\lambda = 532$ nm. In (a), the scattering from 98 nm, 155 nm, and 205 nm spheres are shown for $\theta_i = \theta_s = 45°$. In (b), the scattering from 205 nm spheres for $\theta_i = \theta_s = 30°$, $\theta_i = \theta_s = 45°$, and $\theta_i = \theta_s = 60°$. The solid curves represent the predictions of the BV theory.

One can perform a similar analysis for in-plane data. Figure 7(b) shows the value of η extracted from the data for the 45°-polarized incident light at an angle 20° from the specular direction. In Fig. 5, this value appears to depend upon the particle size, the theory agrees well with the data, and there is little interference from the specularly reflected light. Indeed, comparison between the BV theory and the data allows one to estimate the particle sizes with an uncertainty on the order of a few nanometers. Improvements in the measurement and using multiple scattering angles should reduce the uncertainty in the measured sphere size using these polarized light scattering methods.

5. SUMMARY

The scattering of light by copper and gold spheres on silicon surfaces were measured, and the results were compared to the theory of Bobbert and Vlieger for a sphere on a surface. The measurements establish the validity of our implementation of the BV theory. Comparisons of the BV theory with two approximate theories demonstrate the need to use the more accurate theory for scattering from metallic spheres. Furthermore, it was shown that the existence of any ultrathin film must be included in the calculation in order to obtain accurate results. Two different methods were described for extracting the diameters of these spheres from experimental data.

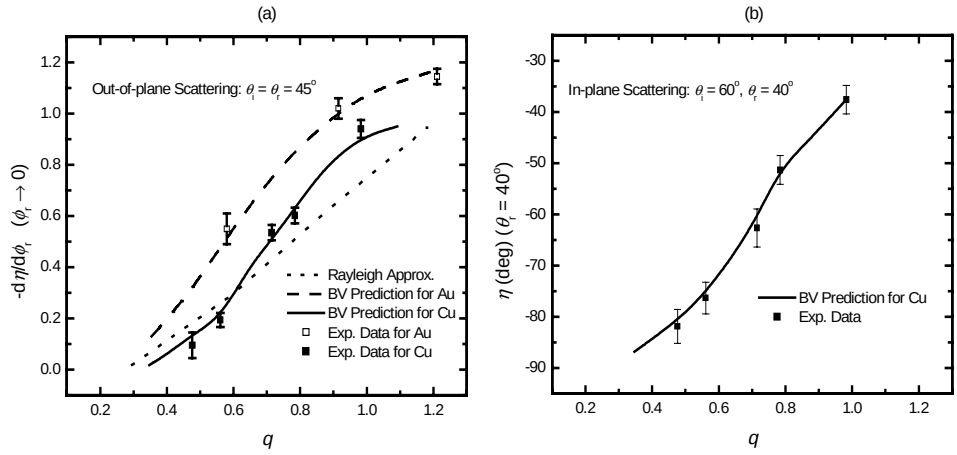

Figure 7. (a) The initial slope $-d\eta/d\phi_r$ extrapolated from out-of-plane measurements to zero azimuthal angle ($\phi_r \to 0$), as a function of the size parameter ($q = 2\pi r/\lambda$) for copper and gold spheres. The curves represent the BV theory and the Rayleigh appoximation. (b) The principal angle of polarization η measured for copper spheres in the plane of incidence ($\theta_i = 60°$, $\theta_r = 40°$, and $\phi_r = 0$) using 45° polarized $\lambda = 633$ nm incident light. The solid curve represents the BV theory.

ACKNOWLEDGEMENTS

The authors would like to thank Mr. Marco Fernandez for assisting in the setup of the copper particle generation equipment, Dr. Jeeseong Hwang for useful comments on the gold particle deposition method, and Mr. Quynh Nguyen for help with the transmission electron microscope.

REFERENCES AND NOTES

1. J. C. Stover, *Optical Scattering: Measurement and Analysis*, (SPIE Optical Engineering Press, Bellingham, WA, 1995).

2. K. B. Nahm and W. L. Wolfe, "Light-scattering models for spheres on a conducting plane: comparison with experiment," Appl. Opt. **26,** 2995–2999 (1987).

3. P. R. Spyak and W. L. Wolfe, "Scatter from particulate-contaminated mirrors. part 1: theory and experiment for polystyrene spheres and l=0.6328 µm," Opt. Eng. **31,** 1746–1756 (1992).

4. G. W. Starr and E. D. Hirleman, "Comparison of Experimentally Measured Differential Scattering Cross Sections of PSL Spheres on Flat Surfaces and Patterned Surfaces," in *Flatness, Roughness, and Discrete Defect Characterization for Computer Disks, Wafers, and Flat Panel Displays,* J. C. Stover, Ed., Proc. SPIE, **2862**, 130–138 (1996).

5. L. Sung, G. W. Mulholland, and T. A. Germer, "Polarized light-scattering measurements of dielectric spheres upon a silicon surface," Opt. Lett. **24,** 866–868 (1999).

6. Y. A. Eremin, J. C. Stover, and N. V. Orlov, "Modeling scatter from silicon wafer features based on discrete sources method," Opt. Eng. **38,** 1296–1304 (1999).

7. D. C. Weber and E. D. Hirleman, "Light scattering signatures of individual spheres on optically smooth conducting surfaces," Appl. Opt. **27,** 4019–4026 (1988).

8. R. Schmehl, B. M. Nebeker, and E. D. Hirleman, "Discrete-dipole approximation for scattering by features on surfaces by means of a two-dimensional fast Fourier transform technique," J. Opt. Soc. Am. A **14,** 3026–3036 (1997).

9. T. A. Germer, "Angular dependence and polarization of out-of-plane optical scattering from particulate contamination, subsurface defects, and surface microroughness," Appl. Opt. **36,** 8798–8805 (1997).

10. T. A. Germer and C. C. Asmail, "Polarization of light scattered by microrough surfaces and subsurface defects," J. Opt. Soc. Am. A **16,** 1326–1332 (1999).

11. T. A. Germer, C. C. Asmail, and B. W. Scheer, "Polarization of out-of-plane scattering from microrough silicon," Opt. Lett. **22,** 1284–1286 (1997).

12. P. A. Bobbert and J. Vlieger, "Light scattering by a sphere on a substrate," Physica **137A,** 209–242 (1986).

13. G. Videen, "Light scattering from a sphere on or near a surface," J. Opt. Soc. Am. A **8,** 483–489 (1991).

14. G. Videen, "Light scattering from a sphere on or near a surface: errata," J. Opt. Soc. Am. A **9,** 844–845 (1992).

15. P. A. Bobbert, J. Vlieger, and R. Greef, "Light reflection from a substrate sparsely seeded with spheres—comparison with an ellipsometric experiment," Physica **137A,** 243–257 (1986).

16. C. F. Bohren and D. R. Huffman, *Absorption and Scattering of Light by Small Particles*, (Wiley, New York, 1983).

17. W. H. Press, B. P. Flannery, S. A. Teukolsky, and W. T. Vetterling, *Numerical Recipes in C: The Art of Scientific Computing*, (Cambridge University, 1991).

18. T. A. Germer, *SCATMECH: Polarized Light Scattering C++ Class Library* (http://physics.nist.gov/scatmech, 2000).

19. J. H. Kim, T. A. Germer, G. W. Mulholland, and S. H. Ehrman, "Decomposition study of copper precursors by spray pyrolysis," to be submitted (2001).

20. P. D. Kinney, D. Y. H. Pui, G. W. Mulholland, and N. P. Bryner, "Use of the electrostatic classification method to size 0.1 µm SRM particles—a feasibility study," J. Res. Natl. Inst. Stand. Technol. **96,** 147 (1991).

21. The uncertainties quoted in this article were obtained by estimating the standard uncertainty s for the measurement and multiplying by a coverage factor of $k = 2$. These values correspond to a confidence level of 95 %.

22. E. D. Palik, *Handbook of Optical Constants of Solids*, (Academic, San Diego, 1985).

23. Certain commercial equipment, instruments, or materials are identified in this paper in order to specify the experimental procedure adequately. Such identification is not intended to imply recommendation or endorsement by the National Institute of Standards and Technology, nor is it intended to imply that the materials or equipment identified are necessarily the best available for the purpose.

24. K. C. Grabar, P. C. Smith, M. D. Musick, J. A. Davis, D. G. Walter, M. A. Jackson, A. P. Guthrie, and M. J. Natan, "Kinetic control of interparticle spacing in Au colloid-based surfaces: Rational nanometer-scale architecture," J. Am. Chem. Soc. **118,** 1148 (1996).

25. W. Kern and D. A. Puotinen, "Cleaning solutions based on hydrogen peroxide for use in silicon semiconductor technology," RCA Review **30,** 187–206 (1984).

26. S. Wolf and R. N. Tauber, *Silicon Processing for the VLSI Era*, (Lattice Press, Sunset Beach, 1987), Vol. 1: Process Technology.

27. T. A. Germer and C. C. Asmail, "A goniometric optical scatter instrument for bidirectional reflectance distribution function measurements with out -of-plane and polarimetry capabilities," in *Scattering and Surface Roughness*, Z.-H. Gu and A. A. Maradudin, Eds., Proc. SPIE, **3141**, 220–231 (1997).

28. T. A. Germer and C. C. Asmail, "Goniometric optical scatter instrument for out-of-plane ellipsometry measurements," Rev. Sci. Instr. **70,** 3688–3695 (1999).

29. F. Zenhausern, Y. Martin, and H. K. Wickramasinghe, "Scanning Interferometric Apertureless Microscopy: Optical Imaging at 10 Angstrom Resolution," Science **269,** 1083–1085 (1995).

30. Girard C., Joachim C., and S. Gauthier, "The physics of the near-field," Rep. Prog. Phys. **63,** 893–938 (2000).